JVI Journals.ASM.org

Establishment and Characterization of a Lethal Mouse Model for the Angola Strain of Marburg Virus

Xiangguo Qiu,[a] Gary Wong,[a,b] Jonathan Audet,[a,b] Todd Cutts,[c] Yulian Niu,[d] Stephanie Booth,[d] Gary P. Kobinger[a,b,e,f]

Special Pathogens Program, National Microbiology Laboratory, Public Health Agency of Canada, Winnipeg, Manitoba, Canada[a]; Department of Medical Microbiology, University of Manitoba, Winnipeg, Manitoba, Canada[b]; Applied Biosafety and Research Program, JC Wilt Infectious Diseases Research Centre, Public Health Agency of Canada, Winnipeg, Manitoba, Canada[c]; Molecular PathoBiology, National Microbiology Laboratory, Public Health Agency of Canada, Winnipeg, Manitoba, Canada[d]; Department of Immunology, University of Manitoba, Winnipeg, Manitoba, Canada[e]; Department of Pathology and Laboratory Medicine, University of Pennsylvania School of Medicine, Philadelphia, Pennsylvania, USA[f]

ABSTRACT

Infections with Marburg virus (MARV) and Ebola virus (EBOV) cause severe hemorrhagic fever in humans and nonhuman primates (NHPs) with fatality rates up to 90%. A number of experimental vaccine and treatment platforms have previously been shown to be protective against EBOV infection. However, the rate of development for prophylactics and therapeutics against MARV has been lower in comparison, possibly because a small-animal model is not widely available. Here we report the development of a mouse model for studying the pathogenesis of MARV Angola (MARV/Ang), the most virulent strain of MARV. Infection with the wild-type virus does not cause disease in mice, but the adapted virus (MARV/Ang-MA) recovered from liver homogenates after 24 serial passages in severe combined immunodeficient (SCID) mice caused severe disease when administered intranasally (i.n.) or intraperitoneally (i.p.). The median lethal dose (LD_{50}) was determined to be 0.015 50% $TCID_{50}$ (tissue culture infective dose) of MARV/Ang-MA in SCID mice, and i.p. infection at a dose of 1,000× LD_{50} resulted in death between 6 and 8 days postinfection in SCID mice. Similar results were obtained with immunocompetent BALB/c and C57BL/6 mice challenged i.p. with 2,000× LD_{50} of MARV/Ang-MA. Virological and pathological analyses of MARV/Ang-MA-infected BALB/c mice revealed that the associated pathology was reminiscent of observations made in NHPs with MARV/Ang. MARV/Ang-MA-infected mice showed most of the clinical hallmarks observed with Marburg hemorrhagic fever, including lymphopenia, thrombocytopenia, marked liver damage, and uncontrolled viremia. Virus titers reached 10^8 $TCID_{50}$/ml in the blood and between 10^6 and 10^{10} $TCID_{50}$/g tissue in the intestines, kidney, lungs, brain, spleen, and liver. This model provides an important tool to screen candidate vaccines and therapeutics against MARV infections.

IMPORTANCE

The Angola strain of Marburg virus (MARV/Ang) was responsible for the largest outbreak ever documented for Marburg viruses. With a 90% fatality rate, it is similar to Ebola virus, which makes it one of the most lethal viruses known to humans. There are currently no approved interventions for Marburg virus, in part because a small-animal model that is vulnerable to MARV/Ang infection is not available to screen and test potential vaccines and therapeutics in a quick and economical manner. To address this need, we have adapted MARV/Ang so that it causes illness in mice resulting in death. The signs of disease in these mice are reminiscent of wild-type MARV/Ang infections in humans and nonhuman primates. We believe that this will be of help in accelerating the development of life-saving measures against Marburg virus infections.

Infections with filoviruses cause severe hemorrhagic fevers with high mortality rates. The family *Filoviridae* is divided into three genera, *Ebolavirus*, *Marburgvirus*, and *Cuevavirus*. Within the *Ebolavirus* genus, Zaire ebolavirus (Ebola virus [EBOV]) is the most pathogenic in humans, with a case fatality rate of up to 90%, followed by the Sudan (54%) and Bundibugyo (34%) ebolaviruses. Together, ebolaviruses have been responsible for more than 1,500 deaths since their discovery in 1976 (1). In contrast, live cuevavirus has not yet been isolated from insectivorous bats (2) and is not known to cause illness in humans, whereas outbreaks of Marburg virus (MARV) have been responsible for fewer than 400 deaths since its discovery in 1967 (3). Although MARV is a less visible threat to humans in terms of total number of outbreaks and deaths, it should be noted that one of the largest and deadliest filovirus outbreaks in history was caused by MARV. An outbreak of the Angolan variant of MARV (MARV/Ang) in Uige, Angola, from 2004 to 2005 resulted in 227 deaths out of 252 total cases, a 90% mortality rate (4). This rate is similar to that of the most devastating EBOV outbreak on record, and MARV/Ang infections currently account for over half of all documented MARV cases and deaths (3).

The development of a mouse-adapted virus for modeling EBOV infections in mice (5) has provided an economical and efficient method for the screening of candidate vaccines and post-

Received 7 June 2014 Accepted 14 August 2014
Published ahead of print 20 August 2014
Editor: S. Perlman
Address correspondence to Xiangguo Qiu. xiangguo.qiu@phac-aspc.gc.ca, or Gary P. Kobinger, gary.kobinger@phac-aspc.gc.ca.
Supplemental material for this article may be found at http://dx.doi.org/10.1128/JVI.01643-14.

doi:10.1128/JVI.01643-14

exposure therapies. Several promising strategies from these experiments have also demonstrated efficacy in higher animal models, highlighted by the vesicular stomatitis virus-based vaccine (VSVΔG/EBOVGP) (6) in addition to monoclonal antibody cocktails (ZMAb and MB-003) (7, 8, 9, 10). However, the number of promising prophylactics and therapeutics against MARV infections has lagged behind its EBOV counterpart, likely due in part to the lack of a widely available rodent-adapted virus that recapitulates MARV disease.

A rodent-adapted Ravn virus (RAVV) was developed previously to address this need. RAVV, a virus within the *Marburgvirus* genus, was first adapted to severe combined immunodeficient (SCID) mice (11) and then in immunocompetent BALB/c mice (12). Sequential passaging of the Musoke and Ci67 variants of MARV (MARV/Mus and MARV/Ci67, respectively) in SCID mice has also yielded lethal host-adapted variants in SCID mice (11); however, it is unknown whether the mouse-adapted MARV/Mus and MARV/Ci67 are also lethal to immunocompetent mice. Complicating matters further, these adapted viruses are not yet widely available for use among biosafety level 4 (BSL-4) laboratories. Additionally, RAVV has 21% nucleotide divergence from MARV/Mus, whereas MARV/Ang is 7% divergent from MARV/Mus based on a whole-genome analysis (11). The glycoprotein (GP) gene shows 22% divergence between RAVV and MARV/Ang in both nucleotide and amino acid sequences (4), suggesting that vaccines and therapeutics raised against RAVV GP may not be protective against MARV challenge and vice versa. Indeed, studies have shown that vaccines based on Venezuelan equine encephalitis virus (VEEV) expressing the GP and nucleoprotein from MARV/Mus are protective against homologous virus challenge in cynomolgus macaques (13) but not protective against a RAVV challenge (14), indicating that the differences between the two virus lineages are sufficient to negatively impact the efficacy of potential candidate vaccines.

There is a need to develop MARV models for immunocompetent small animals using variants that are antigenically distinct from RAVV. This is important for facilitating the development of MARV vaccines or therapeutics so that they can first be tested in small animals with a high predictability of protective efficacy, before follow-up studies in a higher animal species such as nonhuman primates (NHPs). A guinea pig-adapted MARV/Ang variant has been previously described (15); however, sequence data for this MARV variant is not available. The aim of this study was to adapt MARV/Ang, the MARV variant that is most pathogenic in humans, to immunocompetent mice such that a challenge with a sufficient dose will kill the host within days. Here, we describe the development and characterization of a mouse-adapted virus (MARV/Ang-MA) for use in the immunocompetent BALB/c mouse. The adapted virus is characterized with regard to different inoculation routes, various clinical parameters, cytokine, chemokine, and growth factor responses, and the pathology within the various organs during the course of disease. MARV/Ang-MA was also sequenced and compared to the full-length MARV/Ang sequence, in order to distinguish the molecular differences between the two viruses.

MATERIALS AND METHODS

Ethics statement. All animal work was performed according to animal use document (AUD) H-11-007, which has been approved by the Animal Care Committee (ACC) based at the Canadian Science Center for Human and Animal Health (CSCHAH), in accordance with the guidelines outlined by the Canadian Council on Animal Care (CCAC). All infectious work was performed in the biosafety level 4 (BSL-4) facility at the National Microbiology Laboratory in Winnipeg, Canada.

Cells and viruses. The wild-type virus was Marburg virus, strain Angola (Marburg virus H.sapiens-tc/AGO/2005/Angola), termed MARV/Ang, which was isolated from a patient during the 2005 Marburg outbreak in Uige, Angola. The adapted virus is designated Marburg virus NML/M.musculus-lab/AGO/2005/Ang-MA-P2 (MARV/Ang-MA). Stocks of MARV/Ang and MARV/Ang-MA were grown in T-150 flasks (Corning) of Vero E6 cells (ATCC) for use in the studies.

Animals and virus adaptation process. Severe combined immunodeficient (SCID) and wild-type BALB/c mice, female, 4 to 6 weeks old (Charles River), were used for these studies. For passaging experiments, two SCID mice were initially injected intraperitoneally (i.p.) with $\sim 10^6$ PFU of MARV/Ang in 200 μl of Dulbecco's modified Eagle's medium (DMEM), supplemented with 2% heat-inactivated fetal bovine serum (FBS) (Sigma). Serial passaging of MARV/Ang in SCID mice was then performed as follows. Livers were removed from euthanized mice at 7 days postinfection (dpi), pooled, and then homogenized by hand by grinding the livers against a steel mesh with a plastic plunger. The cells were suspended in 10 ml of phosphate-buffered saline (PBS) and centrifuged at 400 × *g* for 5 min. The supernatant was passed through a cell strainer, and the cell pellet was further mechanically homogenized with a tissue homogenizer. After centrifugation at 400 × *g* for 5 min, the supernatant was also passed through the cell strainer. Two naive SCID mice were injected i.p. with 200 μl of the liver homogenate, and the process was repeated again at 7 dpi until a MARV/Ang variant (termed MARV/Ang-MA) lethal to both SCID and BALB/c mice was produced after 24 passages. The virus was not plaque purified.

LD_{50} challenge and pathogenesis experiments. For the median lethal dose (LD_{50}) studies, 10-fold dilutions of MARV/Ang-MA ranging between 2.72×10^{-3} to 2.72×10^{1} $TCID_{50}$ (50% tissue culture infective dose) was administered per SCID or BALB/c mouse (3 or 4 per dilution). The mice were weighed daily and monitored for survival, weight loss, and clinical signs of disease. For the pathogenesis experiments, groups of 10 C57BL/6 mice were given 2,000× LD_{50} (100 $TCID_{50}$) of MARV/Ang-MA i.p., whereas groups of 10 BALB/c mice were administered 2,000× LD_{50} of MARV/Ang-MA i.p., intramuscularly (i.m.), intranasally (i.n.), or subcutaneously (s.c.). Mice were weighed daily and monitored for survival, weight loss, and clinical signs of disease.

Serial sampling experiments. BALB/c mice were infected with either 2,000× LD_{50} of MARV/Ang-MA or an equivalent titer of MARV/Ang. Four to 6 mice from each group were randomly chosen to be euthanized at planned time points between 0 and 6 dpi for necropsy. Blood was sampled from anesthetized mice by retro-orbital bleeding. Whole blood was collected in K2 EDTA plus blood collection tubes (BD Biosciences) for blood counts and determination of viremia and in SST plus blood collection tubes (BD Biosciences) for blood biochemistry studies. Whole blood from mice was also collected in EDTA plus blood collection tubes and spun at 1,000 × *g* for 10 min at 4°C in order to isolate plasma for cytokine responses. Parts of organs, including liver, spleen, kidney, lung, brain, and intestine, were also harvested, weighed, put in 1 ml of DMEM supplemented with 2% heat-inactivated FBS, and then homogenized in a tissue homogenizer. Samples were then spun at 400 × *g* for 5 min and frozen at −80°C until processing. For histopathological and immunohistochemical analyses, whole livers and spleens were harvested from mice and fixed in 10% phosphate-buffered formalin in the BSL-4 laboratory for at least 28 days before processing.

Blood counts and blood biochemistry. Complete blood counts were performed with a VetScan HM5 hematology system (Abaxis Veterinary Diagnostics). The following parameters were included in the results: levels of white blood cells (WBC) and lymphocytes (LYM), percentages of lymphocytes (LY%), monocytes (MO%), and neutrophils (NE%), and levels of platelets (PLT). Blood biochemistry analysis was performed with a

VetScan VS2 analyzer (Abaxis Veterinary Diagnostics). The following parameters were included in the results: levels of alkaline phosphatase (ALP), alanine aminotransferase (ALT), amylase (AMY), total bilirubin (TBIL), blood urea nitrogen (BUN), and glucose (GLU).

Cytokine, chemokine, and growth factor responses. Mouse cytokine, chemokine, and growth factor levels were quantified with the Cytokine Mouse 20-Plex panel for the Luminex platform (Life Technologies) and performed according to the manufacturer's instructions. The following parameters were included in the results: fibroblast growth factor (FGF-basic), gamma interferon (IFN-γ), interleukin-1β (IL-1β), IL-2, IL-4, IL-5, IL-6, IL-10, IL-12, IL-13, IL-17, IFN-γ induced protein 10 (IP-10), keratinocyte chemoattractant (KC), monocyte chemoattractant protein 1 (MCP-1), monokine induced by IFN-γ (MIG), macrophage inflammatory protein 1α (MIP-1α), tumor necrosis factor α (TNF-α), and vascular endothelial growth factor (VEGF).

Infectious virus titrations. Titration of live MARV/Ang or MARV/Ang-MA was performed as follows. Whole blood or supernatants from harvested organs were first serially diluted 10-fold in DMEM supplemented with 2% heat-inactivated FBS. One-hundred-microliter volumes of the dilutions were then added in three replicates to a 96-well plate (Corning) of preseeded Vero E6 cells at 95% confluence and incubated at 37°C for 1 h. The samples were removed, and 100 μl of fresh DMEM with 2% FBS was added to the wells and incubated for 14 days. The plates were scored for the presence of cytopathic effects (CPE) at 14 dpi, and titers were calculated by the Reed and Muench method (16) and expressed as $TCID_{50}$/ml or $TCID_{50}$/g of tissue. The lower detection limit for this assay is 10 $TCID_{50}$/ml or 10 $TCID_{50}$/g of tissue.

Histology and immunohistochemistry. For histology studies, fixed liver and spleen tissues were embedded in paraffin wax to make paraffin blocks. The blocks were then cut 5 μm thick, mounted on Superfrost microscope slides (Fisher), and incubated overnight at 37°C, deparaffinized with two changes of xylene, immersed in 100%, 90%, and then 70% ethanol for 2 min each, washed with distilled water, and then stained with hematoxylin (Thermo Scientific) and eosin Y (Thermo Scientific) for 2 min and 30 s, respectively, with a 2-min wash of distilled water in between. The sections were then dehydrated with 70%, 90%, and 100% ethanol, cleared in two changes of xylene, and mounted with Permount (Fisher) for viewing by routine light microscopy.

For immunohistochemistry studies, paraffin blocks were deparaffinized and washed with distilled water as described above. Sections were first incubated with 10 mM sodium citrate buffer, pH 6.8, at 100°C for 10 min with a NxGen decloaking chamber (Inter Medico) before immunohistochemistry was performed with an UltraVision Quanto mouse on mouse horseradish peroxidase (HRP) kit (Thermo Scientific) in a Lab Vision autostainer (Thermo Scientific) in accordance with the manufacturer's instructions. The in-house monoclonal antibody 3H1, which recognizes MARV GP, was used at a 1:1,000 dilution as a primary antibody.

Statistical analysis. Statistical comparisons of the blood biochemistry data, blood counts, and cytokine data were carried out using R v3.1.1 (17) along with the reshape2 (18), ggplot2 (19), and car (20) packages. The data used for the analysis consisted of 6 parameters for the blood biochemistry data, 8 parameters for the blood counts, and 20 parameters for the cytokines. Only data from days on which both groups were sampled were used. In order to account for the number of comparisons, three multiple analysis of covariance assays (MANCOVAs) were used, one for the biochemistry data, one for the blood count data, and one for the cytokine data. For the purposes of statistical testing, the time variable was considered categorical with 4 values: 1, 3, 5, and 6 (three for the cytokines, namely 3, 5, and 6). In all cases, the MANCOVAs were significant and were followed by individual analysis of covariance assays (ANCOVAs) for each outcome. In the case where the ANCOVA result was significant, a posttest consisting of Tukey's honest significant differences was used to compare the viruses at different times. The assumption of homoscedasticity was tested for each outcome using Levene's test. For the blood biochemistry data, all outcomes except GLU showed heteroscedasticity so a log transformation was used on all outcomes, including GLU, in order to keep the scales consistent. After the transformation, AMY data still showed significant heteroscedasticity and a number of transformations were attempted (see output in the supplemental material), but none corrected the problem. As a consequence, weights ($1/y^2$) were applied to the regression to compensate for the increased impact of the highly variable values. For the blood count data, all outcomes passed Levene's test, so no transformations were applied. For the cytokine data, all cytokines were heteroscedastic and three (IFN-γ, GM-CSF, and IL-1β) were still heteroscedastic after a log transformation. The source of heteroscedasticity for those samples appeared to be groups in which all or most measurements were at background level; because there are no well-documented alternatives to the ANCOVA procedure, we elected to analyze those cytokines in the same manner but the *P* values obtained were interpreted more conservatively. Scripts and output are provided in the supplemental material. For all analyses, statistical significance was set at a *P* value of <0.05. A *P* value of <0.05 was considered significant, a *P* value of <0.01 was considered very significant, and a *P* value of <0.001 was considered extremely significant.

Sequencing of MARV/Ang-MA. RNA was extracted from wild-type and mouse-adapted virus stocks using a Qiagen QIAmp viral RNA mini-kit, per the manufacturer's instructions. The reverse transcription (RT) was carried out using an Improm II kit (Promega). Three different RT reactions were carried out for each virus, and each reaction contained every third forward primer from Table S1 in the supplemental material (e.g., reaction 1 included primers MARV-1F, MARV-4F, MARV-7F, etc.). The two rounds of PCR were carried out using Phusion Green high-fidelity DNA polymerase (Thermo Scientific) in 50-μl reaction mixtures. The first PCR was performed with 2 μl of the RT reaction mixture as the template. Three PCRs per sample were performed combining all the primers in Table S1 in the supplemental material that have the same "reaction ID." The second-round PCR was carried out using the same primers (see Table S2 in the supplemental material for a list of the primer pairs). The second round of PCR used 1 μl of the first-round PCR mixture as the template. The cycling conditions for both rounds were initial denaturation at 98°C for 3 min, followed by 35 cycles of denaturation at 98°C for 30 s, annealing at 55°C for 30 s, and extension at 72°C for 2 min and then a final extension at 72°C for 10 min. The second-round reaction mixtures were run on a 1% agarose gel with SYBR Safe DNA gel stain (Life Technologies), and the PCR products of the appropriate size were purified using a QIAquick gel extraction kit (Qiagen). The samples were sent to an in-house sequencing service. The primers used for sequencing consisted of the amplification primers and all the primers that bind in-between them; e.g., for the product of MARV-3F and MARV-57R, the sequencing primers were MARV-3F, -4F, -5F, -59R, -58R, and -57R. The sequences were assembled in DNAStar Lasergene 9 SeqMan using GenBank sequence DQ447660.1 as the reference sequence.

Nucleotide sequence accession number. The sequence of MARV/Ang-MA was deposited in GenBank under accession number KM261523.

RESULTS

Adaptation of MARV/Ang to SCID and BALB/c mice. Since infection with MARV/Ang does not cause disease in mice, the virus was first passaged in SCID mice using an adaptation protocol that is similar to previously published studies (11). With each passage, the SCID mice got progressively sicker until death was observed by passage 24. The mouse-adapted MARV/Ang (MARV/Ang-MA) was first tested to determine the LD_{50} in SCID mice. Intraperitoneal (i.p.) infection with MARV/Ang-MA caused rapid weight loss in the animals that eventually died, resulting in uniform lethality within 8 days postinfection (dpi) at a dose of 2.72×10^{-1} $TCID_{50}$ or higher of MARV/Ang-MA, 67% (2 of 3) mortality at a dose of 2.72×10^{-2} $TCID_{50}$, and 33% (1 of 3) mortality at a dose

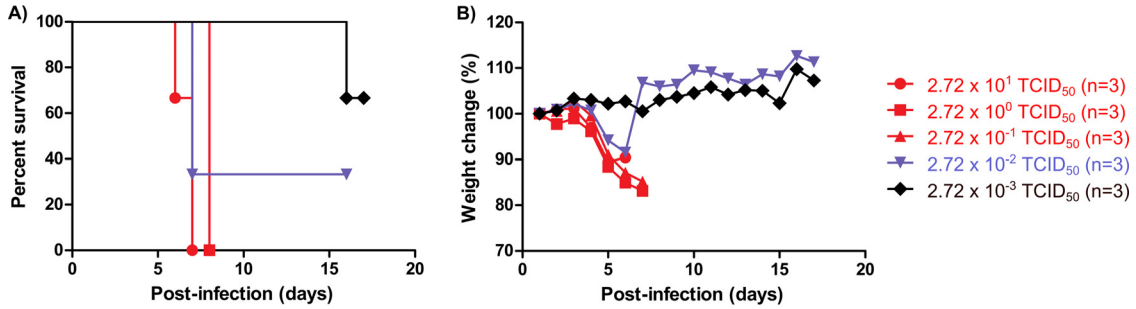

FIG 1 LD_{50} determination of MARV/Ang-MA in SCID mice. SCID mice ($n = 3$) were infected i.p. with 10-fold serial dilutions of MARV/Ang-MA. Survival (A) and weight change (B) were monitored daily for 18 days, and the survivors were kept for up to 28 days after challenge. The LD_{50} was calculated to be 0.015 $TCID_{50}$.

of 2.72×10^{-3} $TCID_{50}$ (Fig. 1A and B). The LD_{50} was calculated to be 1.5×10^{-2} $TCID_{50}$ of MARV/Ang-MA for SCID mice.

Lethal challenge of MARV/Ang-MA in immunocompetent BALB/c and C57BL/6 mice. MARV/Ang-MA was then tested in BALB/c mice in order to determine whether the adapted virus is also lethal to immunocompetent mice without the need for further passaging. Infection of BALB/c mice i.p. also caused rapid weight loss in the animals that eventually died and resulted in uniform lethality within 8 dpi at a dose of 2.72×10^{-1} $TCID_{50}$ or higher of MARV/Ang-MA, 25% (1 of 4) mortality at a dose of 2.72×10^{-2} $TCID_{50}$, and no mortality at a dose of 2.72×10^{-3} $TCID_{50}$ (Fig. 2A and B). The LD_{50} was calculated to be 5×10^{-2}

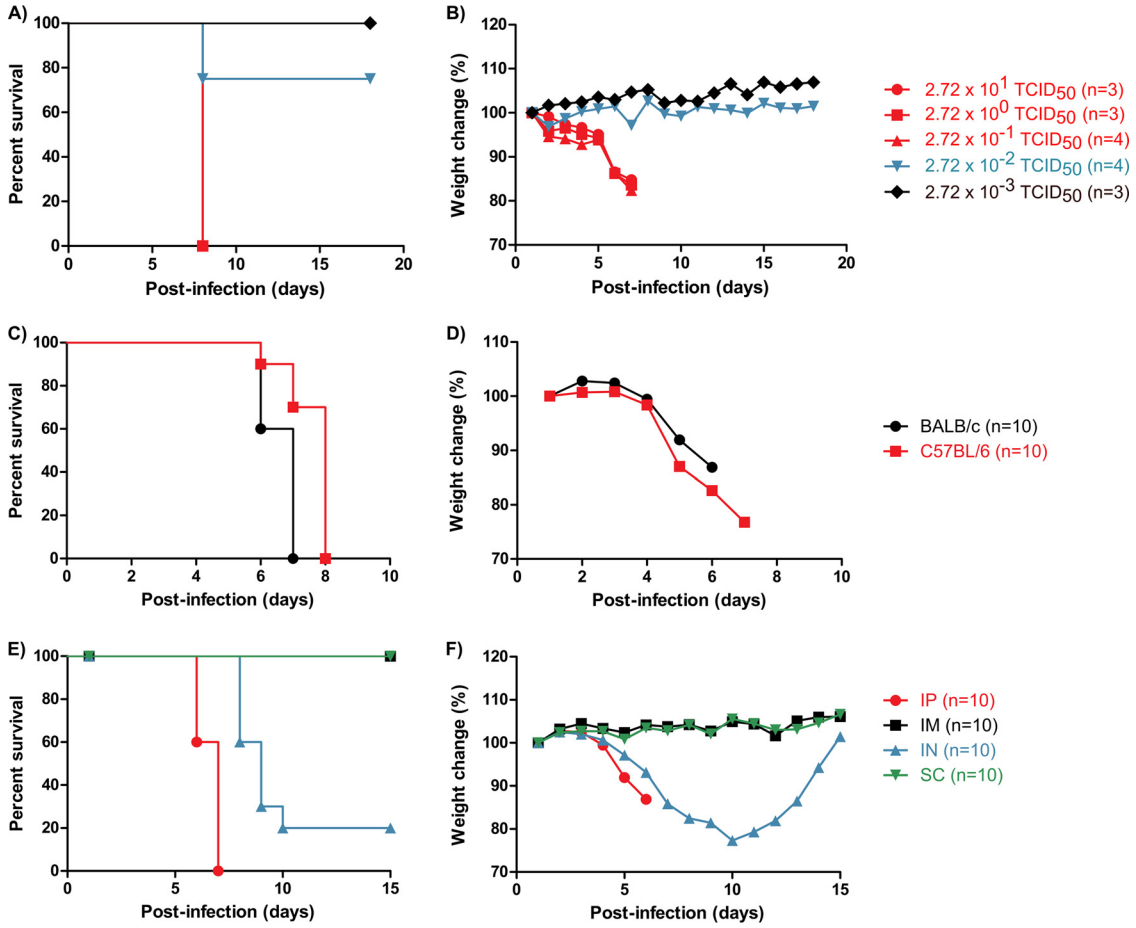

FIG 2 Survival and weight change in immunocompetent mice infected with MARV/Ang-MA. (A and B) BALB/c mice ($n = 3$ or 4) were infected i.p. with 10-fold serial dilutions of MARV/Ang-MA to determine the LD_{50}. Survival (A) and weight change (B) were monitored daily for 18 days, and the survivors were kept for up to 28 days after challenge. The LD_{50} was calculated to be 0.05 $TCID_{50}$. (C and D) To establish a uniformly lethal model of infection in two common wild-type mouse strains, groups of 10 BALB/c or C57BL/6 mice were then infected intraperitoneally (i.p.) with 2,000× LD_{50} of MARV/Ang-MA. Survival (C) and weight change (D) were monitored daily until the termination of the experiment. (E and F) To investigate whether MARV/Ang-MA is lethal via other routes of infection, groups of 10 BALB/c mice were challenged intramuscularly (i.m.), intranasally (i.n.), and subcutaneously (s.c.) with 2,000× LD_{50} of MARV/Ang-MA. Survival (E) and weight change (F) were monitored daily for 15 days, and the survivors were kept for up to 28 days after challenge.

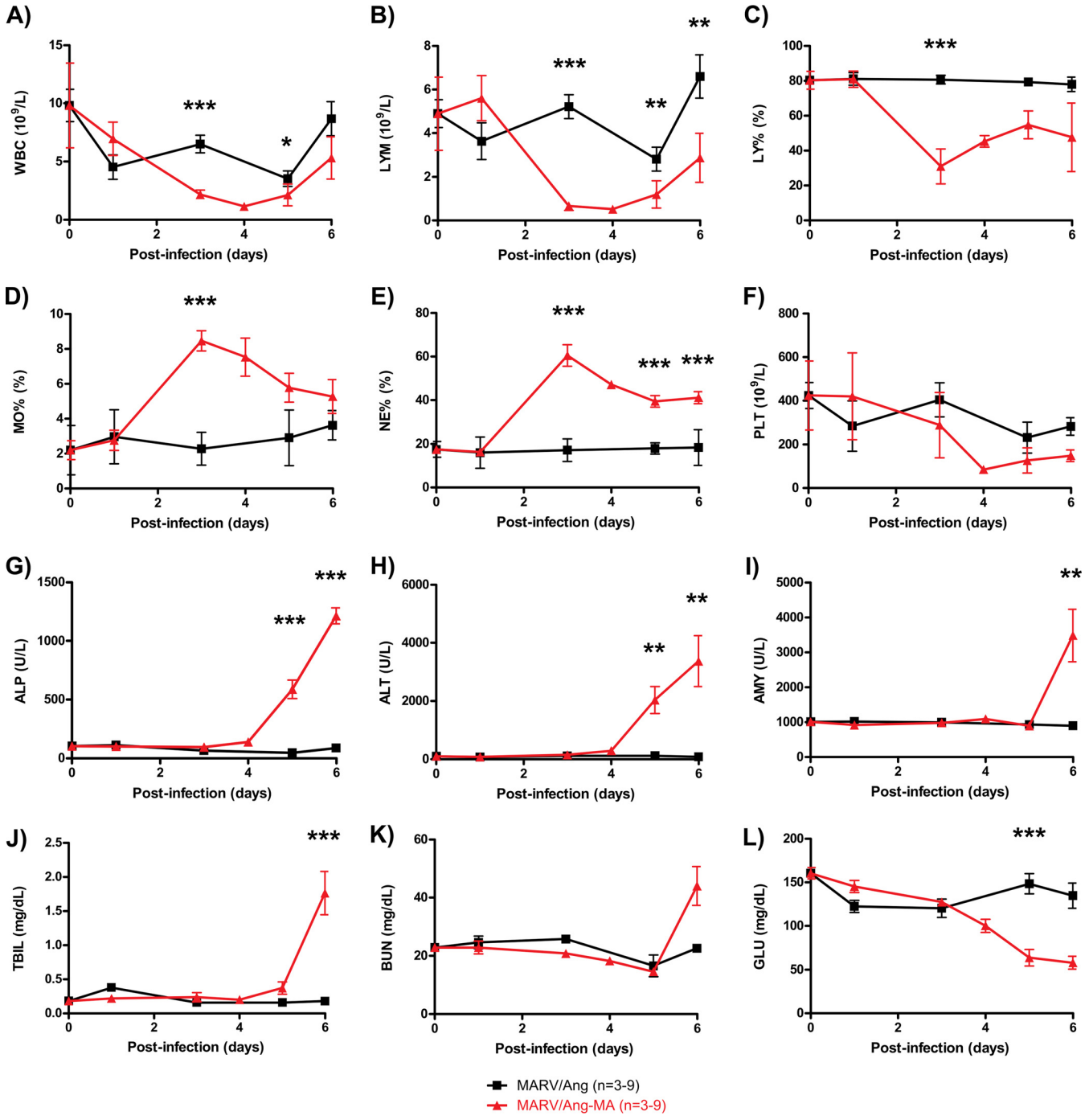

FIG 3 Blood parameters in BALB/c mice infected with MARV/Ang or MARV/Ang-MA. Whole blood and sera were collected at the indicated time points from individual BALB/c mice (3 to 9 per time point) infected with 2,000× LD_{50} MARV/Ang-MA or the equivalent MARV/Ang dose. The whole blood was analyzed with differential, and the following parameters are shown: white blood cell count (WBC) (A), lymphocyte count (LYM) (B), lymphocyte percentage (LY%) (C), monocyte percentage (MO%) (D), neutrophil percentage (NE%) (E), and platelet count (PLT) (F). Sera were analyzed for biochemistry, and the following values are shown: alkaline phosphatase (ALP) (G), alanine aminotransferase (ALT) (H), amylase (AMY) (I), total bilirubin (TBIL) (J), blood urea nitrogen (BUN) (K), and glucose (GLU) (L). The data are expressed as means ± standard errors. *, $P < 0.05$; ** $P < 0.01$; ***, $P < 0.001$ (significance was determined by comparing data for MARV/Ang and MARV/Ang-MA at the same time points).

$TCID_{50}$ of MARV/Ang-MA for BALB/c mice. To establish a uniformly lethal challenge in immunocompetent mice, both BALB/c and C57BL/6 mice were subjected to an i.p. challenge with 2,000× LD_{50} of MARV/Ang-MA. Rapid weight loss was observed in both BALB/c and C57BL/6 mice after infection, and death occurred between 6 and 8 dpi, with a mean time to death (MTD) of 6.6 ± 0.5 and 7.6 ± 0.7 days, respectively (Fig. 2C and D). MARV/Ang-MA challenge by different inoculation routes was also inves-

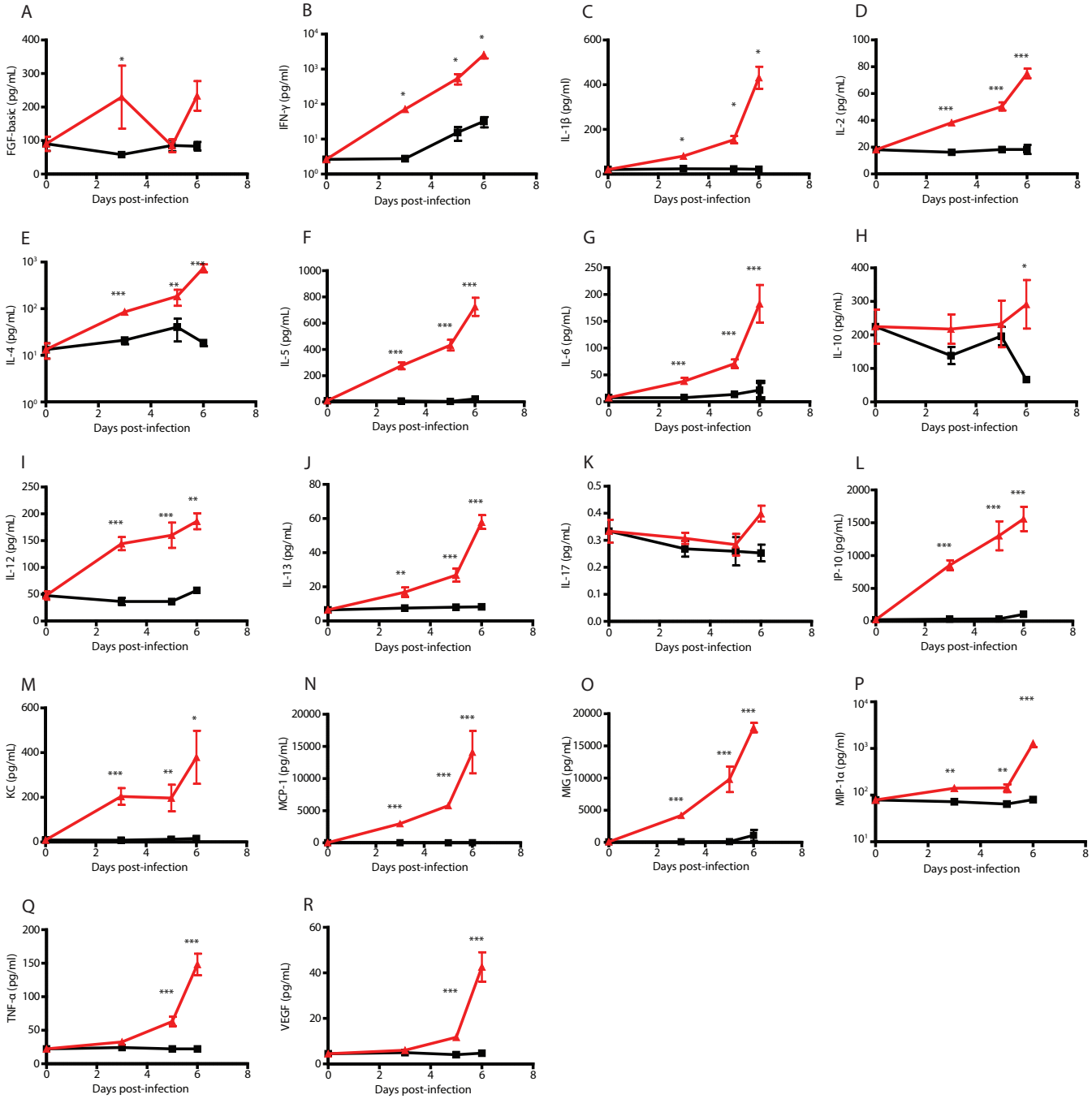

FIG 4 Cytokine, chemokine, and growth factor changes in BALB/c mice infected with MARV/Ang or MARV/Ang-MA. Plasma samples were collected at the indicated time points from individual BALB/c mice (4 to 6 per time point) infected with 2,000× LD_{50} MARV/Ang-MA (red) or the equivalent MARV/Ang (black) dose. The following parameters were presented: FGF-basic (A), gamma interferon (IFN-γ) (B), interleukin-1β (IL-1β) (C), IL-2 (D), IL-4 (E), IL-5 (F), IL-6 (G), IL-10 (H), IL-12 (I), IL-13 (J), IL-17 (K), IFN-γ induced protein 10 (IP-10) (L), keratinocyte chemoattractant (KC) (M), monocyte chemoattractant protein 1 (MCP-1) (N), monokine induced by IFN-γ (MIG) (O), macrophage inflammatory protein 1α (MIP-1α) (P), tumor necrosis factor α (TNF-α) (Q), and vascular endothelial growth factor (VEGF) (R). The data are expressed as means ± standard errors. *, $P < 0.05$; **, $P < 0.01$; ***, $P < 0.001$ (significance was determined by comparing data for MARV/Ang and MARV/Ang-MA at same time points).

tigated in BALB/c mice. Intranasal (i.n.) challenge with 2,000× LD_{50} of MARV/Ang-MA resulted in severe disease in mice and yielded 80% lethality, with a MTD of 8.6 ± 0.7 days. However, intramuscular (i.m.) and subcutaneous (s.c.) challenge with 2,000× LD_{50} of MARV/Ang-MA did not cause disease in BALB/c mice (Fig. 2E and F).

Clinical overview of changes in MARV-infected mice. Changes in hematology and blood biochemistry were determined after infection of BALB/c mice with either 2,000× LD_{50} of MARV/Ang-MA or an equivalent dose of MARV/Ang. As expected, MARV/Ang infection of mice did not cause any notable changes in the tested parameters. In contrast, MARV/Ang-MA infection re-

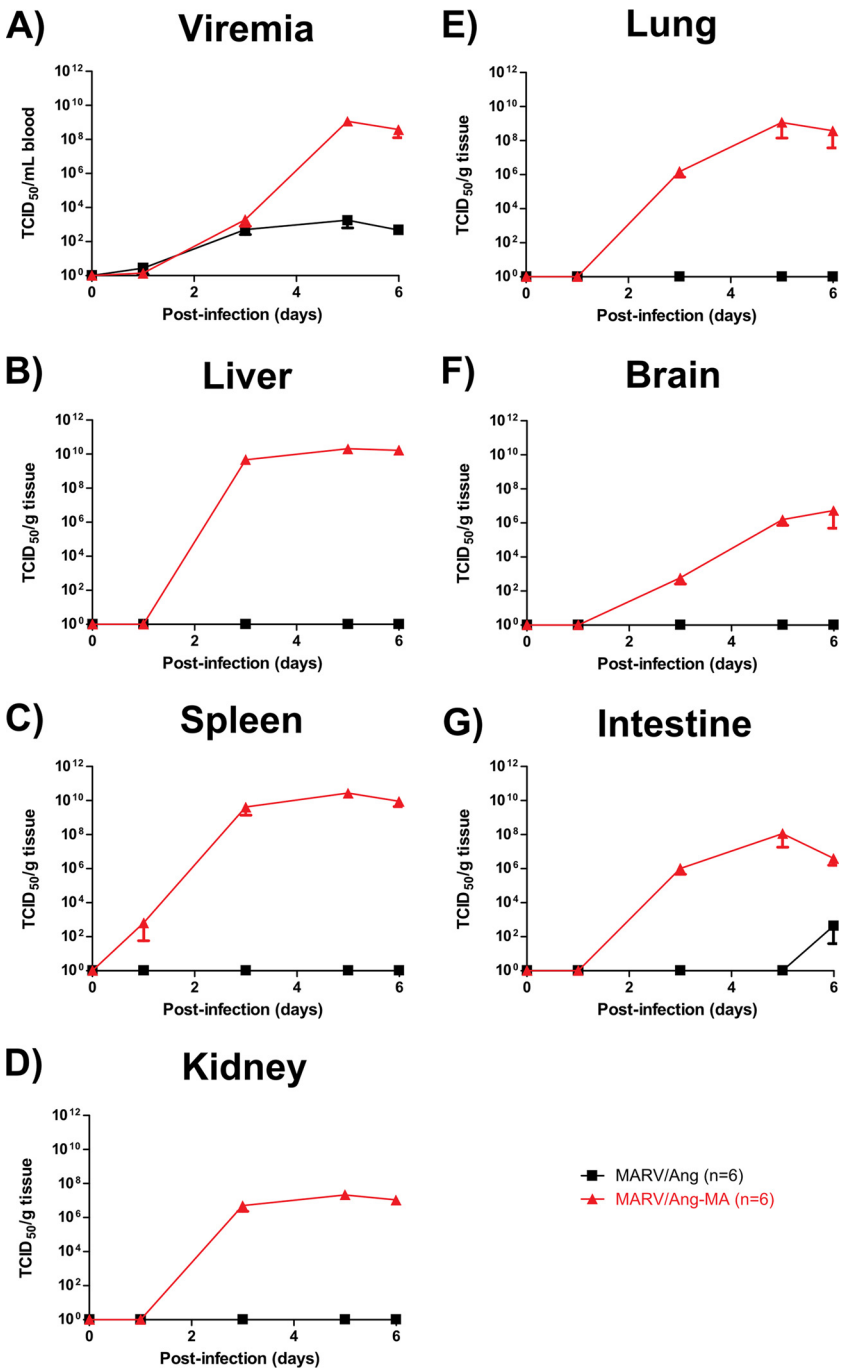

FIG 5 Virus titers in the blood and various tissues of BALB/c mice infected with MARV/Ang or MARV/Ang-MA. Whole blood and tissues were collected from individual BALB/c mice (6 per time point) infected with 2,000× LD_{50} of MARV/Ang-MA or the equivalent MARV/Ang dose. Virus titers in blood (A) or tissue homogenates of liver (B), spleen (C), kidney (D), lung (E), brain (F), and intestine (G) were determined by a $TCID_{50}$ assay. The data are expressed as means ± standard errors.

sulted in a significant decrease in the total white blood cell counts by 3 dpi (Fig. 3A), highlighted by a 10-fold drop in the absolute lymphocyte counts (Fig. 3B) as well as a 50% reduction in percentage of lymphocytes (Fig. 3C). The leukocytopenia was at least partially responsible for the observed increases in monocyte and neutrophil percentages in the MARV/Ang-MA-infected mice (Fig. 3D and E). Platelet counts also decreased in MARV/Ang-MA-infected mice by up to 3-fold over the course of the infection, and this observed thrombocytopenia may be indicative of coagulation disorders (Fig. 3F). Changes in the blood biochemistry parameters of MARV/Ang-MA-challenged mice were detected late, between 5 and 6 dpi. These included elevated levels of the liver enzymes alkaline phosphatase (ALP) and alanine aminotransferase (ALT), increased levels of amylase (AMY), total bilirubin

(TBIL), and blood urea nitrogen (BUN), and a decrease in glucose (GLU) (Fig. 3G and L). The combination of these findings suggests multiorgan failure in these mice, as highlighted by the decrease in liver, pancreas, and kidney functions. Neither rash nor petechiae, a manifestation observed in NHPs infected with MARV/Ang, were seen in the mice at any time after MARV/Ang-MA infection.

Cytokine, chemokine, and growth factor responses in MARV-infected mice. The changes in cytokine, chemokine, and growth factor levels were also measured after the infection of BALB/c mice with either 2,000× LD_{50} of MARV/Ang-MA or an equivalent dose of MARV/Ang. Infection with MARV/Ang did not result in notable changes in most of the tested parameters (Fig. 4A to R). The only exceptions were an upregulation of IFN-γ and a downregulation of IL-10 detected at 5 and 6 dpi, respectively (Fig. 4B and H). In contrast, infection with MARV/Ang-MA resulted in a rapid and significant upregulation of pro- and anti-inflammatory cytokines, chemokines, and growth factors (Fig. 4A to R), which were detectable starting at 3 dpi and increasing until death at 6 dpi.

Biodistribution of MARV/Ang-MA in infected mice. In order to determine the primary organs for MARV/Ang-MA replication in addition to virus spread in the BALB/c mice, MARV/Ang-MA replication was quantified by infectious virus titration at selected time points after infection with the mouse-adapted virus at a dose of 2,000× LD_{50}. Infection with an identical dose of MARV/Ang was used as a control, and evidence of virus replication was investigated in the blood, liver, spleen, kidney, lung, brain, and intestine of each animal. BALB/c mice infected with MARV/Ang had very low viremia, at ~10^2 $TCID_{50}$/ml of blood (Fig. 5A), accompanied by the absence of infectious virus in the tested organs, with the exception of one intestine sample at 6 dpi (Fig. 5B to G). In contrast, BALB/c mice infected with MARV/Ang-MA had high viral loads, reaching ~10^8 $TCID_{50}$/ml of blood by 5 dpi, indicating that systemic spread of the virus had occurred. Indeed, evidence of MARV/Ang-MA infection could be found in all tested tissue samples, with the liver and spleen demonstrating the peak titers of ~10^{10} $TCID_{50}$/g of tissue by 3 dpi. Live MARV/Ang-MA can also be detected starting at 3 dpi in the kidney, lung, brain, and intestine, reaching peak levels of ~10^6, ~10^8, ~10^6 and ~10^8 $TCID_{50}$/g tissue, respectively.

Gross pathology and histopathologic changes in organs of MARV-infected mice. Gross examination of organs from MARV/Ang- and MARV/Ang-MA-infected BALB/c mice at 6 dpi revealed significant pathological differences between the two groups. While the organs of MARV/Ang-infected mice appeared normal, prominent signs of disease can be observed in the MARV/Ang-MA-infected mice, such as intestinal hyperemia (Fig. 6A). Other findings include an enlarged liver and spleen, in addition to discoloration in both the liver and kidneys (Fig. 6B to D).

The livers and spleens were harvested from MARV/Ang- and MARV/Ang-MA-infected animals at various time points after challenge and stained with hematoxylin and eosin to look for histopathological changes. Normal liver morphology was observed in the uninfected mice at day 0. At 3 dpi, acute hepatitis and eosinophilic intracytoplasmic inclusion bodies (ICIBs) in hepatocytes (Fig. 7A, black arrows) were observed. The hepatocytes became swollen, cloudy, ballooned, and distorted; the lobular architecture disappeared, and the cytoplasm showed pallor. At 6 dpi, changes noted at 3 dpi became more prominent, such as extensive

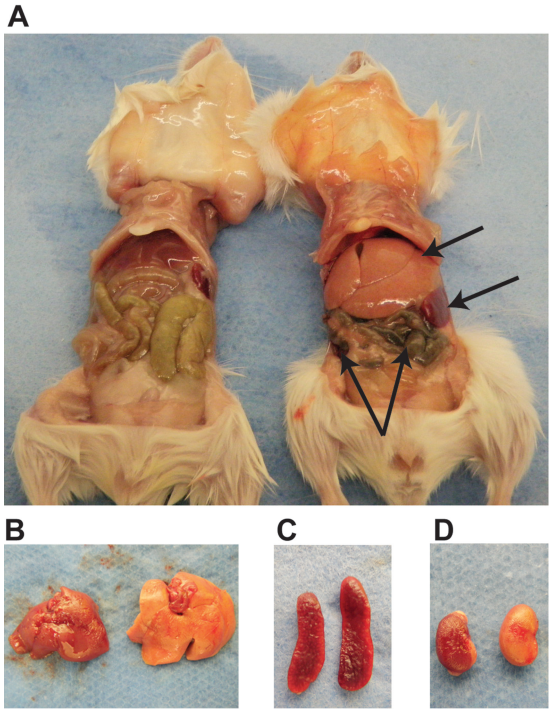

FIG 6 Gross pathology findings in BALB/c mice infected with MARV/Ang or MARV/Ang-MA. (A) *In situ* pictures of organs in a representative MARV/Ang (left)- or MARV/Ang-MA (right)-infected BALB/c mouse at 6 days after infection. Findings include intestinal hyperemia, in addition to an enlarged liver and spleen in the MARV/Ang-MA-infected animal. Discoloration was also observed in the liver and kidney of the MARV/Ang-MA infected animal. Shown are closeup images of liver (B), spleen (C), and kidneys (D), in which the organs infected with the wild-type virus are on the left and those infected with the adapted virus are on the right of each image.

hepatocellular necrosis as well as a large amount of ICIBs (Fig. 7A). Normal splenic morphology was observed at day 0. Mild lymphocyte depletion was noted at 3 dpi in the white pulp, and extensive and severe diffuse necrosis or lymphocyte depletion with the destruction of tissue architecture was observed at 6 dpi (Fig. 7B).

Immunohistochemical staining was also conducted on the livers and spleens of MARV/Ang- and MARV/Ang-MA-infected mice at various time points after challenge. There was no evidence of MARV GP in the livers and spleens sampled at day 0. At 3 dpi, MARV GP was detected in both spleen and liver sections. In livers, MARV GP is apparent primarily on the membrane of hepatocytes at 3 dpi, and the strongest staining was observed on both the membrane and cytoplasm of hepatocytes at 6 dpi (Fig. 8A). In spleens, a small number of cells that were localized in the red pulp stained positive for MARV GP at 3 dpi. The number of cells and the intensity of the staining for MARV GP were much higher at 6 dpi (Fig. 8B).

Sequencing of MARV/Ang-MA. Sequencing of the mouse-adapted virus showed that MARV/Ang-MA contained a total of 11 amino acid changes from MARV/Ang (Table 1), with no frameshift mutations detected. There are 2 mutations in viral protein 35 (VP35), 6 mutations in the major matrix protein VP40, 1 mutation in the glycoprotein, 1 mutation in VP30, and 1 mutation in the minor matrix protein VP24.

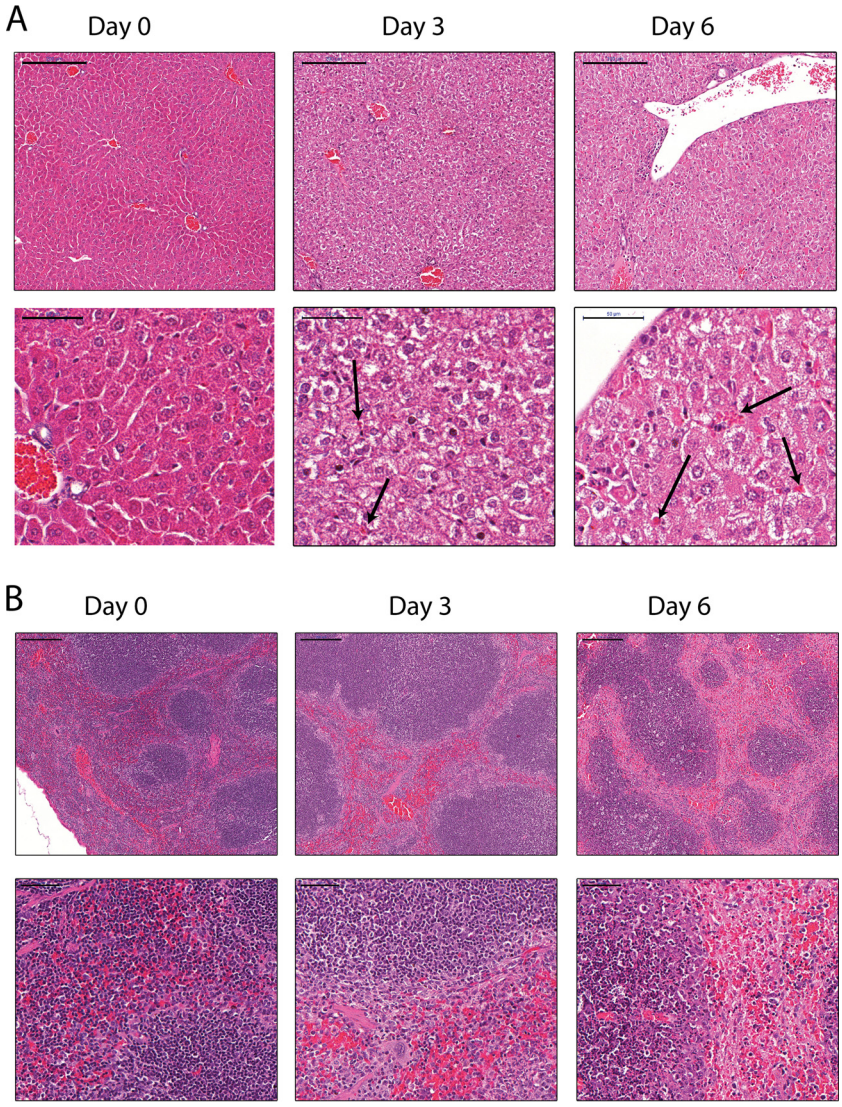

FIG 7 Histopathological changes in the livers and spleens of BALB/c mice infected with MARV/Ang-MA. BALB/c mice ($n = 4$) were infected i.p. with 2,000× LD_{50} of MARV/Ang-MA. Representative pictures of tissues from livers (A) and spleens (B), which were collected at the indicated time points and stained with hematoxylin and eosin, are shown. Top panels are of lower magnification, and bottom panels are of higher magnification (scale bars, 200 and 50 μm, respectively).

DISCUSSION

A novel model was developed for studying MARV/Ang infections in both SCID and immunocompetent mice in which i.p. challenge with MARV/Ang-MA was lethal, with the animals succumbing to challenge within 6 to 8 dpi. The clinical disease produced in BALB/c mice includes high viremia and viral tissue titers, which were detectable starting at 3 dpi until death, profound loss of lymphocytes, platelet decrease, increased liver and pancreatic enzymes, and the accumulation of metabolic wastes. At the end stage of disease, there is evidence of systemic infiltration of virus throughout the host, as indicated by the presence of live MARV/Ang-MA in various organs as detected by determination of $TCID_{50}$, the gross pathological observations of the liver, spleen, kidney, and intestine, and histological and immunohistochemical analyses of the livers and spleens of MARV/Ang-MA-infected mice.

An important aspect of the utility of these rodent-adapted viruses is the predictive accuracy of vaccine and therapeutic efficacy in NHPs stemming from these preliminary studies. From EBOV studies, it has been previously shown that potential vaccines and treatments that are efficacious in rodents are not necessarily predictive in NHPs. For instance, while the administration of inactivated EBOV as a vaccine is 100% protective in mice after 4 weeks (21), only 64% and 10% protection levels were observed in guinea pigs and NHPs after 21 and 11 weeks, respectively (22) (23). Another example is the VEEV-based vaccine, in which 100% protection was achieved by immunization of both mice and guinea pigs when challenged at 8 and 22 weeks, respectively (24), but no protection was conferred to VEEV-immunized NHPs when challenged at 15 weeks (23). On the therapeutic side, administration of the neutralizing antibody KZ52 was fully protective in guinea pigs at 1 h after challenge (25) but did not impact the course of disease

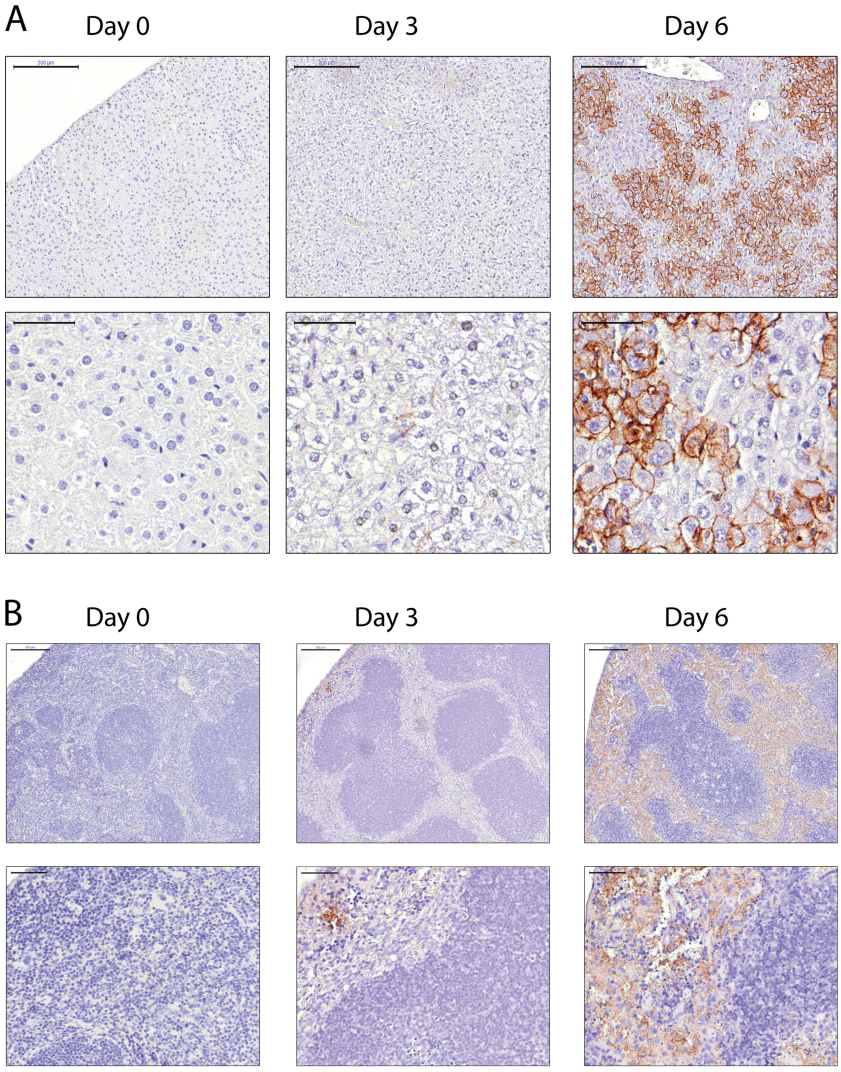

FIG 8 Immunohistochemistry findings in the livers and spleens of BALB/c mice infected with MARV/Ang-MA. BALB/c mice ($n = 4$) were infected i.p. with 2,000× LD_{50} of MARV/Ang-MA. Representative picture of livers (A) and spleens (B), which were collected at the indicated time points and with immunohistochemical staining performed using a monoclonal antibody against the MARV glycoprotein (GP), are shown. Top panels are of lower magnification, and bottom panels are of higher magnification (scale bars, 200 and 50 μm, respectively).

in NHPs when given 24 h before and 96 h after EBOV challenge (26). Additionally, postexposure administration of DEF201 was shown to be 100% efficacious in mice (27), but its use in guinea pigs (28) and NHPs (8) did not result in survival. A potential reason for this discrepancy is that the mouse- and guinea pig-adapted EBOV fails to fully recapitulate all of the hallmarks of EBOV disease in NHPs and humans. For example, while both the mouse and the guinea pig display weight loss, thrombocytopenia, and abnormal cytokine responses after infection with their respective host-adapted EBOV, moribund mice do not show coagulation abnormalities, whereas guinea pigs show only a limited decrease in lymphocyte counts (29). It is hypothesized that this negatively impacts the predictive power of vaccine and treatment efficacy in NHPs and is one of the reasons behind the recent development of a Syrian golden hamster animal model, in which both lymphocyte apoptosis and coagulation disorders can be observed during the course of disease (30). However, whether this animal model is superior to the mouse and guinea pig model in predicting potential vaccine and treatment efficacy remains to be determined.

Pathology studies on MARV/Ang infection in NHPs have been published previously (31). Infection of rhesus macaques i.m. with 1,000 PFU of MARV/Ang results in death by 8 dpi (MTD = 7.3 days), which is similar to the results of MARV/Ang-MA infection of both BALB/c and C57BL/6 mice. Characteristic features of MARV/Ang infection in the NHPs include lymphocytopenia, thrombocytopenia, and elevated levels of circulating enzymes such as ALP, ALT, and TBIL. Livers and spleens had virus titers of $\sim 10^9$ PFU/g tissue, whereas virus titers in other tissues ranged between $\sim 10^5$ and $\sim 10^8$ PFU/g tissue. The liver also showed reticulation and discoloration, hepatocellular degeneration inflammation, and abundant numbers of cells immunopositive for MARV GP antigen at the late stages of disease (31). The observations described above were also seen when BALB/c mice were infected with MARV/Ang-MA. There is very limited information available on the host immunological responses against MARV/

TABLE 1 Summary of all mutations in MARV/Ang-MA compared to MARV/Ang[a]

Region	Nucleotide position	WT	MA	Amino acid change
NP	736	C	T	D→D
NP/VP35 IR	2403	T	C	
	2415	T	C	
	2784	T	C	
	2790	T	C	
	2797	T	C	
	2808	T	C	
	2809	T	C	
	2810	T	C	
	2870	T	C	
	2871	T	C	
	2874	T	C	
	2876	T	C	
	2879	T	C	
	2892	T	C	
	2897	T	C	
	2899	T	C	
	2902	T	C	
	2904	T	C	
	2907	T	C	
	2908	T	C	
	2911	T	C	
	2912	T	C	
	2913	T	C	
	2914	T	C	
	2915	T	C	
	2924	A	G	
	2926	T	C	
VP35	2962	T	C	Y→Y
	2984	T	C	L→L
	3033	T	C	L→S
	3044	T	C	Y→H
VP40	4647	T	C	L→S
	4665	T	C	L→P
	4691	A	C	N→H
	4707	T	C	L→S
	4802	G	A	G→S
	5117	G	A	D→N
VP40/GP IR	5603	T	C	
	5850	A	G	
GP	7204	A	G	N→D
GP/VP30 IR	8378	C	T	
VP30	9175	A	G	N→D
VP24	10675	G	A	V→M
L	14933	G	A	E→E
Trailer	19104	T	A	
	19105	A	G	

[a] WT, wild type (MARV/Ang); MA, MARV/Ang-MA; IR, intergenic region.

Ang infections. Therefore, it is unknown whether the results observed in BALB/c mice infected with MARV/Ang-MA emulate those of NHPs infected with MARV/Ang. However, an uncontrolled systemic release of pro- and anti-inflammatory cytokines, chemokines, and other soluble mediators is a hallmark common to lethal filovirus infections. IFN-α and IL-6 expression has previously been demonstrated in NHPs infected with MARV/Ci67 (32), and *in vitro* studies have shown that infection of monocytes and macrophages with MARV/Mus induces release of IL-6, IL-8, and TNF-α (33) (34).

Data from a published study investigating aerosol infection of NHPs with MARV/Ang are also available (35). Challenge of cynomolgus macaques i.n. with between 99 and 705 PFU of MARV/Ang results in death for all infected animals by 8 dpi, with many of the same clinical signs as those observed in i.m. challenged animals, such as lymphopenia, thrombocytopenia, elevated levels of several chemokines and cytokines, and enlarged friable fatty livers, in addition to fibrous interstitial pneumonia in the lungs (35). While in-depth pathology studies have not yet been performed in BALB/c mice challenged i.n. with MARV/Ang-MA, it will be interesting to see whether the disease observed in those mice will be similar to that in NHPs in the future.

The number of nonsilent mutations in the VP24 and VP35 genes of MARV/Ang-MA compared to that in MARV/Ang indicates that the virus has likely adapted to efficiently escape type I host IFN responses (36) (37); however, it is currently unclear which of these mutations are critical for enhanced virulence in mice. Interestingly, the mutations at nucleotide positions 3044 of VP35 and 5117 of VP40 in our studies were also observed in the mouse-adapted RAVV (12), which suggests that these two mutations may be especially critical for adaptation. It would therefore be important to elucidate the determinants of virulence in MARV/Ang-MA and to investigate whether the same mutations are able to transfer virulence to other previously nonvirulent MARV strains.

NHPs are currently the gold standard animal model for the accurate recapitulation of filovirus disease. For any promising vaccines and treatments to be considered for clinical trials, it must be successful in NHPs. However, due to ethical, practical, and financial considerations, a rodent-based model is a desirable and valuable tool to screen potential vaccines and drugs for efficacy. The development of a mouse-adapted virus opens up many new areas of research, such as mechanistic studies with transgenic knockout mice, in-depth immunology studies, and potentially virus transmission studies, which would otherwise be less practical in NHPs. The murine model should be useful for the BSL-4 scientific community and may play an important role in the discovery and development of improved prophylactics and therapeutics against MARV infections.

ACKNOWLEDGMENTS

We thank Kaylie Tran and Jenna Aviles for their excellent technical assistance.

This work was supported by the Public Health Agency of Canada (PHAC) and funded by a Canadian Safety and Security Program (CSSP) grant to G.P.K. and X.Q. G.W. is the recipient of a Doctoral Research Award from the Canadian Institute for Health Research (CIHR).

We declare no competing interests.

REFERENCES

1. **CDC.** 2014, posting date. Outbreaks chronology: Ebola hemorrhagic fever. Accessed 8 August 2014. http://www.cdc.gov/vhf/ebola/resources/outbreak-table.html.
2. **Negredo A, Palacios G, Vazquez-Moron S, Gonzalez F, Dopazo H, Molero F, Juste J, Quetglas J, Savji N, de la Cruz Martinez M, Herrera JE, Pizarro M, Hutchison SK, Echevarria JE, Lipkin WI, Tenorio A.** 2011. Discovery of an ebolavirus-like filovirus in europe. PLoS Pathog. 7:e1002304. http://dx.doi.org/10.1371/journal.ppat.1002304.

3. **CDC.** January 2014, posting date. Chronology of Marburg hemorrhagic fever outbreaks. Accessed 8 August 2014. http://www.cdc.gov/vhf/marburg/resources/outbreak-table.html.
4. **Towner JS, Khristova ML, Sealy TK, Vincent MJ, Erickson BR, Bawiec DA, Hartman AL, Comer JA, Zaki SR, Stroher U, Gomes da Silva F, del Castillo F, Rollin PE, Ksiazek TG, Nichol ST.** 2006. Marburgvirus genomics and association with a large hemorrhagic fever outbreak in Angola. J. Virol. **80:**6497–6516. http://dx.doi.org/10.1128/JVI.00069-06.
5. **Bray M, Davis K, Geisbert T, Schmaljohn C, Huggins J.** 1998. A mouse model for evaluation of prophylaxis and therapy of Ebola hemorrhagic fever. J. Infect. Dis. **178:**651–661. http://dx.doi.org/10.1086/515386.
6. **Jones SM, Feldmann H, Stroher U, Geisbert JB, Fernando L, Grolla A, Klenk HD, Sullivan NJ, Volchkov VE, Fritz EA, Daddario KM, Hensley LE, Jahrling PB, Geisbert TW.** 2005. Live attenuated recombinant vaccine protects nonhuman primates against Ebola and Marburg viruses. Nat. Med. **11:**786–790. http://dx.doi.org/10.1038/nm1258.
7. **Qiu X, Audet J, Wong G, Pillet S, Bello A, Cabral T, Strong JE, Plummer F, Corbett CR, Alimonti JB, Kobinger GP.** 2012. Successful treatment of Ebola virus-infected cynomolgus macaques with monoclonal antibodies. Sci. Transl. Med. **4:**138ra181. http://dx.doi.org/10.1126/scitranslmed.3003876.
8. **Qiu X, Wong G, Fernando L, Audet J, Bello A, Strong J, Alimonti JB, Kobinger GP.** 2013. mAbs and Ad-vectored IFN-alpha therapy rescue Ebola-infected nonhuman primates when administered after the detection of viremia and symptoms. Sci. Transl. Med. **5:**207ra143. http://dx.doi.org/10.1126/scitranslmed.3006605.
9. **Olinger GG, Jr, Pettitt J, Kim D, Working C, Bohorov O, Bratcher B, Hiatt E, Hume SD, Johnson AK, Morton J, Pauly M, Whaley KJ, Lear CM, Biggins JE, Scully C, Hensley L, Zeitlin L.** 2012. Delayed treatment of Ebola virus infection with plant-derived monoclonal antibodies provides protection in rhesus macaques. Proc. Natl. Acad. Sci. U. S. A. **109:**18030–18035. http://dx.doi.org/10.1073/pnas.1213709109.
10. **Pettitt J, Zeitlin L, Kim DH, Working C, Johnson JC, Bohorov O, Bratcher B, Hiatt E, Hume SD, Johnson AK, Morton J, Pauly MH, Whaley KJ, Ingram MF, Zovanyi A, Heinrich M, Piper A, Zelko J, Olinger GGs.** 2013. Therapeutic intervention of Ebola virus infection in rhesus macaques with the MB-003 monoclonal antibody cocktail. Sci. Transl. Med. **5:**199ra113. http://dx.doi.org/10.1126/scitranslmed.3006608.
11. **Warfield KL, Alves DA, Bradfute SB, Reed DK, VanTongeren S, Kalina WV, Olinger GG, Bavari S.** 2007. Development of a model for marburgvirus based on severe-combined immunodeficiency mice. Virol. J. **4:**108. http://dx.doi.org/10.1186/1743-422X-4-108.
12. **Warfield KL, Bradfute SB, Wells J, Lofts L, Cooper MT, Alves DA, Reed DK, VanTongeren SA, Mech CA, Bavari S.** 2009. Development and characterization of a mouse model for Marburg hemorrhagic fever. J. Virol. **83:**6404–6415. http://dx.doi.org/10.1128/JVI.00126-09.
13. **Hevey M, Negley D, Pushko P, Smith J, Schmaljohn A.** 1998. Marburg virus vaccines based upon alphavirus replicons protect guinea pigs and nonhuman primates. Virology **251:**28–37. http://dx.doi.org/10.1006/viro.1998.9367.
14. **Daddario-DiCaprio KM, Geisbert TW, Geisbert JB, Stroher U, Hensley LE, Grolla A, Fritz EA, Feldmann F, Feldmann H, Jones SM.** 2006. Cross-protection against Marburg virus strains by using a live, attenuated recombinant vaccine. J. Virol. **80:**9659–9666. http://dx.doi.org/10.1128/JVI.00959-06.
15. **Ursic-Bedoya R, Mire CE, Robbins M, Geisbert JB, Judge A, MacLachlan I, Geisbert TW.** 2014. Protection against lethal Marburg virus infection mediated by lipid encapsulated small interfering RNA. J. Infect. Dis. **209:**562–570. http://dx.doi.org/10.1093/infdis/jit465.
16. **Reed LJ, Muench H.** 1938. A simple method of estimating fifty per cent endpoints. Am. J. Hyg. **27:**493–497.
17. **R Development Core Team.** 2011. R: a language and environment for statistical computing, vol 1. R Foundation for Statistical Computing, Vienna, Austria.
18. **Wickham H.** 2007. Reshaping data with the reshape package. J. Stat. Soft. **21:**1–20. http://www.jstatsoft.org/v21/i12.
19. **Wickham H.** 2010. ggplot2: elegant graphics for data analysis, 3rd ed. Springer, New York, NY.
20. **Fox J, Weisberg S.** 2011. An R companion to applied regression, 2nd ed. SAGE Publications, Thousand Oaks, CA.
21. **Rao M, Bray M, Alving CR, Jahrling P, Matyas GR.** 2002. Induction of immune responses in mice and monkeys to Ebola virus after immunization with liposome-encapsulated irradiated Ebola virus: protection in mice requires CD4(+) T cells. J. Virol. **76:**9176–9185. http://dx.doi.org/10.1128/JVI.76.18.9176-9185.2002.
22. **Lupton HW, Lambert RD, Bumgardner DL, Moe JB, Eddy GA.** 1980. Inactivated vaccine for Ebola virus efficacious in guineapig model. Lancet **316:**1294–1295.
23. **Geisbert TW, Pushko P, Anderson K, Smith J, Davis KJ, Jahrling PB.** 2002. Evaluation in nonhuman primates of vaccines against Ebola virus. Emerg. Infect. Dis. **8:**503–507. http://dx.doi.org/10.3201/eid0805.010284.
24. **Pushko P, Bray M, Ludwig GV, Parker M, Schmaljohn A, Sanchez A, Jahrling PB, Smith JF.** 2000. Recombinant RNA replicons derived from attenuated Venezuelan equine encephalitis virus protect guinea pigs and mice from Ebola hemorrhagic fever virus. Vaccine **19:**142–153. http://dx.doi.org/10.1016/S0264-410X(00)00113-4.
25. **Parren PW, Geisbert TW, Maruyama T, Jahrling PB, Burton DR.** 2002. Pre- and postexposure prophylaxis of Ebola virus infection in an animal model by passive transfer of a neutralizing human antibody. J. Virol. **76:**6408–6412. http://dx.doi.org/10.1128/JVI.76.12.6408-6412.2002.
26. **Oswald WB, Geisbert TW, Davis KJ, Geisbert JB, Sullivan NJ, Jahrling PB, Parren PW, Burton DR.** 2007. Neutralizing antibody fails to impact the course of Ebola virus infection in monkeys. PLoS Pathog. **3:**e9. http://dx.doi.org/10.1371/journal.ppat.0030009.
27. **Richardson JS, Wong G, Pillet S, Schindle S, Ennis J, Turner J, Strong JE, Kobinger GP.** 2011. Evaluation of different strategies for post-exposure treatment of Ebola virus infection in rodents. J. Bioterror Biodef. **S1:**007. http://dx.doi.org/10.4172/2157-2526.S1-007.
28. **Qiu X, Wong G, Fernando L, Ennis J, Turner JD, Alimonti JB, Yao X, Kobinger GP.** 2013. Monoclonal antibodies combined with adenovirus-vectored interferon significantly extend the treatment window in Ebola virus-infected guinea pigs. J. Virol. **87:**7754–7757. http://dx.doi.org/10.1128/JVI.00173-13.
29. **Nakayama E, Saijo M.** 2013. Animal models for Ebola and Marburg virus infections. Front. Microbiol. **4:**267. http://dx.doi.org/10.3389/fmicb.2013.00267.
30. **Ebihara H, Zivcec M, Gardner D, Falzarano D, LaCasse R, Rosenke R, Long D, Haddock E, Fischer E, Kawaoka Y, Feldmann H.** 2013. A Syrian golden hamster model recapitulating Ebola hemorrhagic fever. J. Infect. Dis. **207:**306–318. http://dx.doi.org/10.1093/infdis/jis626.
31. **Geisbert TW, Daddario-DiCaprio KM, Geisbert JB, Young HA, Formenty P, Fritz EA, Larsen T, Hensley LE.** 2007. Marburg virus Angola infection of rhesus macaques: pathogenesis and treatment with recombinant nematode anticoagulant protein c2. J. Infect. Dis. **196**(Suppl 2): S372–S381. http://dx.doi.org/10.1086/520608.
32. **Fritz EA, Geisbert JB, Geisbert TW, Hensley LE, Reed DS.** 2008. Cellular immune response to Marburg virus infection in cynomolgus macaques. Viral Immunol. **21:**355–363. http://dx.doi.org/10.1089/vim.2008.0023.
33. **Feldmann H, Bugany H, Mahner F, Klenk HD, Drenckhahn D, Schnittler HJ.** 1996. Filovirus-induced endothelial leakage triggered by infected monocytes/macrophages. J. Virol. **70:**2208–2214.
34. **StroherU, West E, Bugany H, Klenk HD, Schnittler HJ, Feldmann H.** 2001. Infection and activation of monocytes by Marburg and Ebola viruses. J. Virol. **75:**11025–11033. http://dx.doi.org/10.1128/JVI.75.22.11025-11033.2001.
35. **Alves DA, Glynn AR, Steele KE, Lackemeyer MG, Garza NL, Buck JG, Mech C, Reed DS.** 2010. Aerosol exposure to the Angola strain of Marburg virus causes lethal viral hemorrhagic fever in cynomolgus macaques. Vet. Pathol. **47:**831–851. http://dx.doi.org/10.1177/0300985810378597.
36. **Bale S, Julien JP, Bornholdt ZA, Kimberlin CR, Halfmann P, Zandonatti MA, Kunert J, Kroon GJ, Kawaoka Y, MacRae IJ, Wilson IA, Saphire EO.** 2012. Marburg virus VP35 can both fully coat the backbone and cap the ends of dsRNA for interferon antagonism. PLoS Pathog. **8:**e1002916. http://dx.doi.org/10.1371/journal.ppat.1002916.
37. **Valmas C, Basler CF.** 2011. Marburg virus VP40 antagonizes interferon signaling in a species-specific manner. J. Virol. **85:**4309–4317. http://dx.doi.org/10.1128/JVI.02575-10.